MOLECULAR-DYNAMIC SIMULATION ON THE STATICAL AND DYNAMICAL PROPERTIES OF FLUIDS IN A NANO-CHANNEL

Hai Hoang,[1] Sangmo Kang[1] and Yong Kweon Suh*[1]

The equilibrium molecular-dynamic simulations have been performed to estimate the properties of the three kinds of fluids confined between two plates that are separated by 1.086 nm; included in the statical properties are the density distribution and the static structure, and the autocorrelation velocity function in the dynamic property. Three kinds of fluids considered in this study are the Lennard-Jones fluid, water and aqueous sodium-chloride solution. The water molecules are modeled by using the SPC/E model and the ions by the charged Lennard-Jones particle model. To treat the water molecules, we combined the quaternion coordinates with Euler angles. We also proposed a plausible algorithm to assign the initial position and direction of molecules. The influence of polarization of water molecules as well as the presence of ions in the solution on the properties will be addressed in this study. In addition, we performed the non-equilibrium molecular-dynamic simulation to compute the flow velocity for the case with the gravitational force acting on molecules.

Key Words : Molecular-dynamic Simulation, Aqueous sodium-chloride, Water, Lennard-Jones fluid, Nano-channel

1. INTRODUCTION

In recent years, the properties of fluid confined between two plates that are separated by a distance in the range from a few times the diameter of molecules to several nanometers have been studied by using molecular-dynamic(MD hereafter) simulation[1-5]. The characteristics of interaction among fluid molecules themselves and that between fluid and wall molecules as well as the gap between plates strongly affect the structure of fluid, i.e. the local variation of fluid properties, such as the density distribution and the radial distribution function, etc.(However, one exceptional case is for the hydrophobic walls; by using various models for the fluid-wall interaction, Kumar et al.[4] found that the properties of liquid were weakly dependent on the details of confining potential(potential between the wall and the fluid molecules) for the specific case of smooth walls). The effect of the channel gap on these properties was also investigated for both the Lennard-Jones fluid and electrolyte[1-2,6]. With the gap of 1-4 times the diameter of molecules, the fluid showed some anomalous properties such as the equilibrium freezing temperature, solidification, static structure, etc.[4-5]. These properties are different from those of the bulk. Increasing the gap to several nanometers, however, results in the similar properties between the two[2,6-8].

In both MD and Monte Carlo methods, the interaction among the water molecules themselves and that between water and other kinds of molecules are characterized by two kinds of forces. They are the Lennard-Jones force and the electrical force. We may well postulate that both

Received: November 19, 2008, Revised: January 7, 2009, Accepted: January 9, 2009.

1 Department of Mechanical Engineering, Dong-A University

* Corresponding author, E-mail: yksuh@dau.ac.kr

forces are equally important in determining the statical and dynamical properties of fluids. However, there are a few studies in which they only considered the Lennard-Jones force and obtained reasonable results such as the density distribution and the velocity profile[9,10]. This implies that there are some properties of fluid confined within the channel that are weakly influenced by the electrical force.

In previous studies, in order to implement the rigid models such as SPC/E for water molecules, various algorithms like SETTLE, SHAKE and LINCS have been popularly used in MD simulation; these algorithms have also been modified to perform the energy minimization[6-8]. On the other hand, the Euler angle has been utilized to constraint the structure of water molecules[20]. This method is easier for application than the previous algorithms, i.e. SETTLE, SHAKE and LINCS, etc[19,20]. However, this method has never been applied in MD simulation for fluid in a channel even though it was successfully used in the Monte Carlo simulation[11]. The reason for this may be due to difficulty in setting up the initial configuration of molecules including positions and Euler angles in such way that it produces small net force and moment of molecules.

Our main purpose in the present paper is to apply MD simulation in order to investigate the effect of the electrical force and presence of ions in solution on the properties of fluid in a nano-channel for three kinds of fluids. In addition, we propose that the Euler angles combined with quaternion coordinates can be used effectively to constraint the rigid structure of the water molecules. A plausible algorithm is also developed to reasonably perform the initial configuration of all the molecules. In addition, the non-equilibrium MD simulations were performed to estimate the dependence of the flow rate on the pressure gradient as well as the velocity profile across the channel.

2. Molecular-Dynamic Simulation

A. Physical Model

In our study, we treated three kinds of fluids. The first one is the so called Lennard-Jones fluid, in which no electric forces are considered and the coefficients ε and σ for the Lennard-Jones potential.

$$u(r) = 4\varepsilon\left[\left(\frac{\sigma}{r}\right)^{12} - \left(\frac{\sigma}{r}\right)^{6}\right] \tag{1}$$

are the same as those for oxygen, see Table 1. Here, r is the distance between i^{th} and j^{th} molecules. We selected this fluid because it will be more convenient in comparatively investigating the effect of the polarization of water(i.e. the second kind of fluid) on the fluid properties. There are 460 molecules in this case.

As the second fluid, the pure water is modeled by using the SPC/E model, in which the structure is rigid and hydrogen and oxygen are represented by point charges ($q_H = +0.425e$ and $q_O = -0.847e$). The interaction potential among water molecules is constituted by the Lennard-Jones potential acting between the oxygen-site pairs and the electric potential between all pairs of point charges[20]. The number of molecules used in this simulation amounts to 460.

The third fluid is composed of 460 water molecules and 4 pairs of sodium and chloride ions; we will call this 'aqueous sodium-chloride solution' or simply 'solution'. We enforced the Lennard-Jones potential between oxygen sites of water and ion molecules and the electric potential between charged sites of water and ions[20]. Fig. 1 presents an arbitrary distribution of molecules and ions to be subjected to the MD simulation together with the coordinate system.

The channel walls are modeled by two layers of silicon atoms, each layer being oriented in the <100> direction[21](Fig. 1). Typical lateral dimensions of the channels wall are 4.344×4.344 nm which correspond 128 silicon atoms for each layer of channel wall. The walls are separated by 1.086 nm. We considered the interaction between the wall and fluid molecules by using the Lennard-Jones type. The parameters selected for the Lennard-Jones potential(1) are summarized in Table 1.

B. Mathematical Models and Numerical Methods

For each kind of fluids the equations of motions of molecules are different. For the 1st fluid only the translational motion will be considered. For the second and third, rotational motions are additionally considered.

The governing equation for the translational motion of

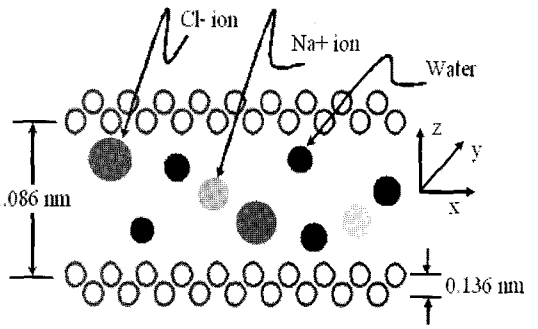

Fig. 1 Schematic of a nano-channel containing water molecules, sodium ions and chloride ions, corresponding to the 3rd kind of fluid treated in this study

the i^{th} molecule is

$$m_i \frac{d}{dt}\mathbf{v}_i = \mathbf{F}_i, \tag{2}$$

where, m_i is the mass of molecule, $\mathbf{v}_i$ is the velocity and $\mathbf{F}_i$ is the total force exerting on the molecule.

To describe the rotational motion for water molecules, we use the Euler angles combined with the quaternion coordinates[16,18]. The governing equation for the rotational motion is

$$\frac{d}{dt}\mathbf{I}^s = \boldsymbol{\tau}^s, \tag{3}$$

where, $\mathbf{I}^s$ is the angular momentum and $\boldsymbol{\tau}^s$ is the torque about the center of mass of the molecule in the space-fixed frame.

Next, the angular momentum in body-fixed frame, $\mathbf{I}^b$ is given as

$$\mathbf{I}^b = [A]\mathbf{I}^s, \tag{4}$$

where [A] is the rotation matrix defined as

$$[A] = \begin{pmatrix} q_0^2+q_1^2-q_2^2+q_3^2 & 2(q_1q_2+q_0q_3) & 2(q_1q_3-q_0q_2) \\ 2(q_1q_2-q_0q_3) & q_0^2-q_1^2+q_2^2-q_3^2 & 2(q_2q_3+q_0q_1) \\ 2(q_1q_3+q_0q_2) & 2(q_2q_3-q_0q_1) & q_0^2-q_1^2-q_2^2+q_3^2 \end{pmatrix} \tag{5}$$

Here, q_m $(m=0,1,2,3)$ indicates the four components of the quaternion $\mathbf{Q}$ that are related to the Euler angles (φ,θ,ϕ) as follows.

$$\begin{aligned} q_0 &= \cos(\theta/2)\cos((\varphi+\phi)/2) \\ q_1 &= \sin(\theta/2)\cos((\varphi-\phi)/2) \\ q_2 &= \sin(\theta/2)\sin((\varphi-\phi)/2) \\ q_3 &= \cos(\theta/2)\sin((\varphi+\phi)/2) \end{aligned} \tag{6}$$

Further, we need the dynamical equation for $\mathbf{Q}$ in terms of the angular velocity components defined in the body-fixed frame $(\omega_x^b, \omega_y^b, \omega_z^b)$:

$$\frac{d}{dt}\begin{pmatrix} q_0 \\ q_1 \\ q_2 \\ q_3 \end{pmatrix} = \frac{1}{2}\begin{pmatrix} q_0 & -q_1 & -q_2 & -q_3 \\ q_1 & q_0 & -q_3 & q_2 \\ q_2 & q_3 & q_0 & -q_1 \\ q_3 & -q_2 & q_1 & q_0 \end{pmatrix}\begin{pmatrix} 0 \\ \omega_x^b \\ \omega_y^b \\ \omega_z^b \end{pmatrix} \tag{7}$$

The leap-frog Verlet algorithm was used to integrate these differential equations with the numerical time step ranging from 1.0 to 3.0 fs depending on the type of fluid as well as the density[18].

There are three kinds of forces acting on each molecule including the Lennard-Jones force $\mathbf{f}_{L-J}$, the Coulomb force $\mathbf{f}_c$ and the external force $\mathbf{f}_e$ encompassing the gravitational or electric force. In general, the total force $\mathbf{F}_i$ acting on the i^{th} molecule can be written as:

$$\mathbf{F}_i = \boldsymbol{f}_{L-J,i} + \boldsymbol{f}_{C,i} + \boldsymbol{f}_{e,i} \tag{8}$$

The first term on RHS of Eq. (8) is computed by

Table 1 Parameters for the Lennard-Jones potential (1)

Interaction	ε(kJ/mol)	σ(nm)
O-O	0.645	0.317
O-Si	1.262	0.327
O-Cl	0.538	0.375
O-Na	0.200	0.286
Cl-Cl	0.445	0.445
Cl-Si	1.044	0.388
Cl-Na	0.166	0.339
Na-Na	0.062	0.257
Na-Si	0.398	0.295

following formula:

$$\mathbf{f}_{L-J,i} = 24\varepsilon_{ij} \sum_{\mathbf{n}\in Z^2} {}^{*} \sum_{j} \left[2\left(\frac{\sigma_{ij}}{s_{ij}}\right)^{12} - \left(\frac{\sigma_{ij}}{s_{ij}}\right)^{6} \right] \times \frac{\mathbf{s}_{ij}}{s_{ij}^2} \qquad (9)$$

where, $\mathbf{s}_{ij} = \mathbf{r}_{ij} + n_x L_x \mathbf{e}_x + n_y L_y \mathbf{e}_y$, and $s_{ij} = |\mathbf{s}_{ij}|$. Further, $\mathbf{e}_x$ and $\mathbf{e}_y$ are unit vectors, $\mathbf{n} = (n_x, n_y)$ a pair of integers, and L_x and L_y denote the spatial size of the physical domain. Here the superscript * indicates the omission of the term with $i = j$ when $\mathbf{n} = 0$. This double summation is effectively computed by applying the minimum-image criterion, cut-off and neighbor algorithm[18-19]. A cutoff radius of 0.8 nm and a neighbor radius of 1.1 nm are used in this study.

The Coulomb force, i.e. the second term on RHS of Eq. (8), can be obtained from

$$\mathbf{f}_{C,i} = q_i \sum_{\mathbf{n}\in Z^2} {}^{*} \sum_{j} \frac{q_j}{s_{ij}^2} \frac{\mathbf{s}_{ij}}{s_{ij}} \qquad (10)$$

where q_i denotes the charge of the i^{th} molecule. The 3D Ewald-summation can not be directly applied for this double summation, because there is no periodicity in the z-direction(see Fig. 1). This problem can be overcome by using an equivalent model and adding the correction term[15]. First, we have elongated the simulation domain in the z-direction by adding a vacuum space of 12 nm. With this special treatment, we can apply the periodic boundary conditions for all directions. The effect of such artificial slabs added to the physical slab is insignificant, because the vacuum space is large. Second, we must add correction terms. Thus, Eq. (10) is effectively computed as follows[12,15].

$$\mathbf{f}_{C,i} = \mathbf{f}_{C,i}^{(r)} + \mathbf{f}_{C,i}^{(k)} + \mathbf{f}_{C,i}^{(c)} \qquad (11)$$

Each of the RHS terms are called the real-space, Fourier-space and correction forces, respectively, to be determined by

$$\mathbf{f}_{C,i}^{(r)} = q_i \sum_{j} q_j \sum_{\mathbf{n}\in Z^3} {}^{*} \left(\frac{2\alpha}{\sqrt{\pi}} exp(-\alpha^2 s'^2_{ij}) + \frac{erfc(\alpha s'_{ij})}{s'_{ij}} \right) \frac{\mathbf{s}'_{ij}}{s'^2_{ij}} \qquad (12)$$

$$\mathbf{f}_{C,i}^{(k)} = \frac{q_i}{V} \sum_{j} q_j \sum_{\mathbf{k}\neq 0} \frac{4\pi \mathbf{k}}{k^2} exp\left(-\frac{k^2}{4\alpha^2}\right) \sin(\mathbf{k} \cdot \mathbf{r}_{ij}) \qquad (13)$$

$$\mathbf{f}_{C,i}^{(c)} = \left(-\frac{4\pi q_i}{V} \sum_{j} q_j z_j \right) \mathbf{e}_z \qquad (14)$$

where, $\mathbf{s}'_{ij} = \mathbf{r}_{ij} + n_x L_x \mathbf{e}_x + n_y L_y \mathbf{e}_y + n_z L_{z,new} \mathbf{e}_z$, $s'_{ij} = |\mathbf{s}'_{ij}|$, $V = L_x L_y L_{z,new}$, α is the splitting parameter of the Ewald sum having the dimension of inverse of length, which controls the relative importance of contributions coming from the real and reciprocal space(Fourier space), and the vector $\mathbf{k}$ is the discrete set $(2\pi/L_x, 2\pi/L_y, 2\pi/L_{z,new}) Z^3$.

The first term on the RHS of Eq. (11) rapidly falls to zero with the distance s'_{ij}, so we selected a cutoff radius of 1.1 nm and a neighbor radius of 1.4 nm. The second term was effectively computed by applying the PPPM method(Particle-Particle-Particle-Mesh)[13,14]. In this method, an FFT grid spacing of 0.12 nm and a TSC(triangular shaped cloud, 2nd order) for the charge distribution and the force interpolation were chosen. We assume that the performance of the charge assignment and the force interpolation can be improved by using the minimum-image criterion, the cut-off and the neighbor list methods. The third term of Eq. (11) contributes to Coulomb force from the z-component of the total dipole moment of the simulation slab[15].

The last term of Eq. (8) is the external force which is considered only for the non-equilibrium molecular-dynamic simulations. In this study, we considered only the gravity force.

To avoid the viscous heating, the Berendsen thermostat was used with the time constant 0.1 ps[7,18]. Then velocities were rescaled as follows

$$\mathbf{v}_{new} = \chi \mathbf{v}_{old} \qquad (15)$$

where the rescaling parameter χ reads

$$\chi = \left[1 - \frac{\Delta t}{\tau} \left(\frac{T_{desire}}{T} - 1 \right) \right]^{1/2} \qquad (16)$$

Here T_{desire} is a desired temperature, i.e. 300K and T is

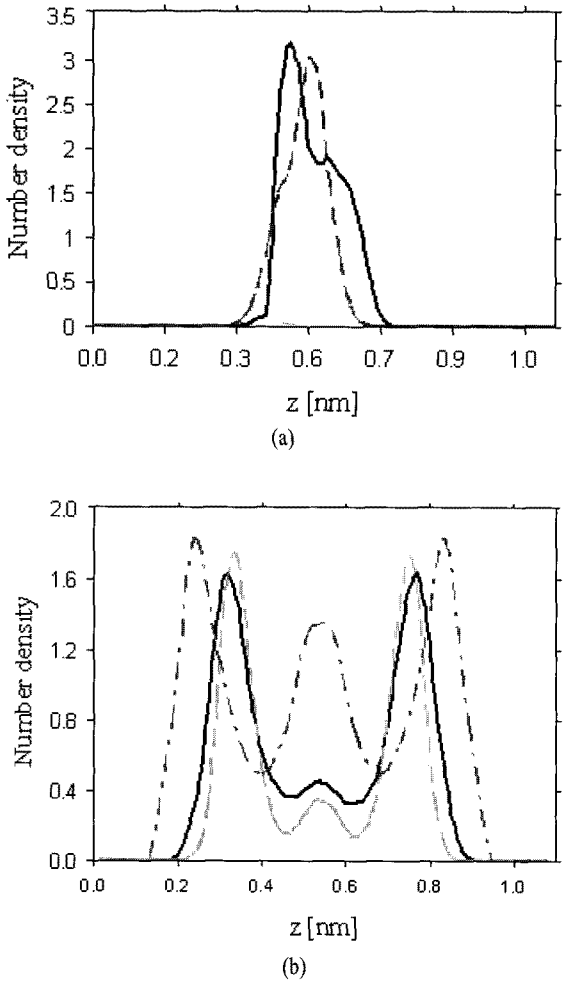

Fig. 2 The number density profile of each molecule along z-direction in the channel; In (a), fluid, respectively. In (b), the solid and long-dash curves indicate the chloride and sodium ions, respectively

the temperature at (t-Δt/2) to be calculated from the general formula for the rigid molecule:

$$fNk_BT=\sum_{i=1}^{N}\left[m_i v_i^2+\omega_i^b \cdot \mathbf{I} \cdot \omega_i^b\right] \tag{17}$$

where, $\mathbf{I}$ is the moment of inertia tensor, f is the number of degrees of freedom(e.g, six for the water molecules and three for other molecules), k_B is the Boltzmann's constant, N is the number of molecules. The temperature T was calculated self consistently with three iterations. In non-equilibrium molecular-dynamic simulations, there is non-trivial streaming flow along the channel, so the motion of molecules is constituted from two types; one is the streaming motion and the other the thermal motion. However, the streaming velocity is so small compared to the velocity by the thermal motion. Hence, we neglected the influence of the streaming velocity in determining the thermal kinetic energy.

Before starting the MD simulation, the initial positions, orientation, translational and rotational velocities of all the molecules have to be assigned. The velocities are chosen randomly from a Gaussian distribution, which are corrected so that no overall linear momentum is produced; also magnitudes that should contribute to the half of the set-up temperature 300K. We set up the rotational velocities for each water molecule in a similar way. We set the values randomly and being corrected so that there is no overall angular momentum, and contributing again to the half of the temperature at 300K[18].

We used the Euler angles combined with quaternion coordinates to describe the motion of rigid water molecules, so we must pay attention in setting the initial positions and orientations of molecules such that the intermolecular force and the torque should not be so large. By using the energy minimization[6,8], we could set up a configuration that reveals reasonably small interaction forces. However, even for small forces, the system may independently show large interaction torques. So we proposed a plausible algorithm to avoid large torque. Firstly, all molecules were assigned with random positions and orientations. While keeping the orientations of the water molecules we performed the energy minimization to find the initial positions having small forces. The steepest descent method combined with the conjugate gradient method was applied in this energy minimization. To implement the line minimization, we used the Brent method and parabolic interpolation[17] with the spatial step size for the line search 0.01nm. After this first step, we can get a configuration with small interaction force, but the interaction moment can be large. In order to reduce the torque we add damping terms to Eqs. (2) and (3). Then, the equations of motions become

$$m_i\frac{d}{dt}\mathbf{v}_i=\mathbf{F}_i-\alpha_F\mathbf{v}_i \tag{18}$$

$$\frac{d}{dt}\mathbf{I}^s = \boldsymbol{\tau}^s - \alpha_T \mathbf{I}^s \tag{19}$$

where α_F and α_T are the damping coefficients for the force and the moment, respectively. In our study, we chose α_F=0.732 N·ps/m and α_T=19.22 ps^{-1}. We set zero as the initial values for integration of Eqs. (18) and (19). The above processes were performed in a subspace (i.e. a quarter space in the (x,y) plane) following the idea of [7]. After that, we copied the set-up obtained in this way to all the other subspaces for use as the initial conditions for the MD simulation.

In the non-equilibrium molecular-dynamic simulation, we applied the gravity force in the x-direction. The gravity force acting on a molecule varied from 68 to 406 fN(typically a factor of 10^8). The reason for application of such high gravity force is that since the interactive force between molecules themselves and that between the wall and molecules is so large; hence, the statistical error becomes so high if the actual gravity force were applied.

To reach the steady state, the system was simulated for the time duration 0.4-0.8 ns. After the system reached the steady state, we performed sampling every 10 time steps in order to compute the average statistics for 0.3-1 ns except for the velocity autocorrelation functions(VACF). For the VACF, the sampling was performed every 10 time steps for 0.05 ns. The binning method was used to compute the density and velocity profile across the channel.

3. Results and Discussion

As the first step, the equilibrium MD simulation has been performed. We present the numerical results of the density profile, the radial distribution function and the velocity autocorrelation function obtained in this simulation.

A. Density Profiles

The number density is defined as:

$$\rho(n) = \frac{1}{A\triangle z M}\sum_{j=1}^{M}\sum_{i=1}^{N} H_n(z_{i,j}) \tag{20}$$

$$H_n(z_{i,j}) = 1 \text{ if } (n-1)\triangle z < z_{i,j} < n\triangle z \tag{21}$$

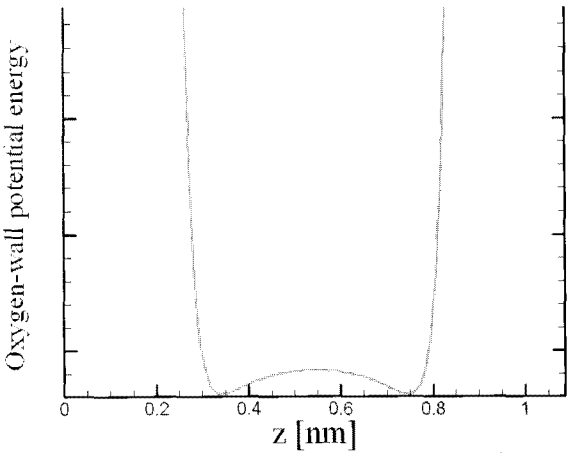

Fig. 3 The Lennard-Jones potential of the wall-oxygen interaction as a function of the position(z-coordinate) of the water molecule

where M is the numbers of samples and N is the number of particles. The repulsive interaction between the wall and the fluid molecules result in the space adjacent to wall that is devoid of the fluid molecules. So, the effective range L'_z normal to the wall accessible to the fluid molecules was quantified as

$$L'_z = L_z - 2\delta \tag{22}$$

where, δ is approximately a gap of the space adjacent to wall. In this paper, we evaluated the gap δ equal to 0.16, 0.3 and 0.3 nm for the Lennard-Jones fluid, the water fluid and the aqueous sodium-chloride solution cases, respectively[3]. This leads to the effective number density

$$\rho_{eff} = \frac{N}{L_x L_y L_z'} \tag{23}$$

The number density profiles of the Lennard-Jones molecules and the center of mass of the water molecules in the pure water fluid and in the solution are shown in Fig. 2(a), while those of the sodium ions and chloride ions in Fig. 2(b). All the number densities were normalized with their effective number densities.

Fig. 2(a) shows three maximum peaks with one lowest peak in the mid-channel which indicates three-layer structure in the channel, composed of the two layers with

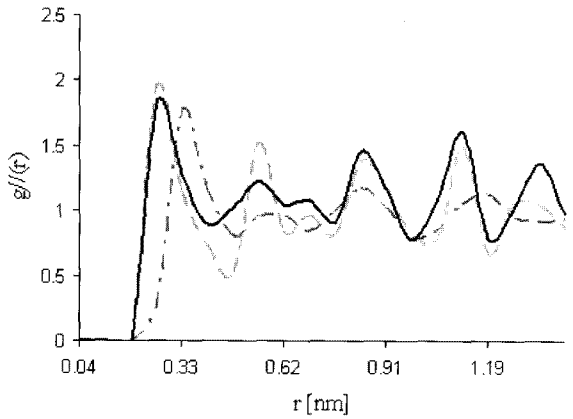

Fig. 4 The lateral radial distribution function g//(r)of the molecules of the Lennard-Jones fluid and the center of water molecular mass of the pure water and the solution in the plane parallel to the wall; long dash, solid and dash dot lines are for water, solution and Lennard-Jones fluids, respectively

highest peaks close to the walls(referred to as 'first layer' hereafter) and one mid-layer with lower peaks. Positions of the first layers in both the water fluid and the aqueous sodium-chloride solution are further away from the wall than those in the Lennard-Jones fluid, which means that for the water fluid and the aqueous sodium-chloride solution the channel surface is more hydrophobic than that for Lennard-Jones fluid. Such difference is possibly due to the influence of the electric force. The two first layers are mainly formed by the fluid-wall interaction, which can be understood by looking into the Lennard-Jones potential between fluid and wall molecules as shown in Fig. 3. These layers show high density and affect the behavior of molecules in the mid-channel playing the role of virtual walls.

We see from Fig. 2(a) that the first-layer peaks show almost the same height for the three fluids. However, the peaks in the mid-channel are quite different. Compared with the case of the Lennard-Jones fluid, the cases with the water fluid and aqueous sodium-chloride solution show much lower peaks in the mid-channel. This can be understood by the influence of the gap between the two first layers; that is we expect that the potential energy for the case of Lennard-Jones fluid having a larger gap may be lower than the case of the other fluids having a smaller gap. Further, Fig. 2(a) shows that the number density profiles in the water fluid and the aqueous sodium-chloride solution are not largely different from each other. This implies that the effect of the presence of ions on this property is not considerable.

Fig. 2(b) shows the number density profile for the sodium and chloride ions. We see that those ions only concentrate in the mid-channel because of the formation of two water layers close to walls as mentioned previously. The distributions are however asymmetric contrary to our expectation, which is obviously caused by the statistical error due to a relatively short time of integration; the sampled time corresponds to 0.4 ns but we have spent almost one week in obtaining these results.

B. Radial Distribution Function

In the previous section, we considered the density distribution in the z-direction; from this result, we can get in formation about the structure of liquid, i. e. density distribution across the channel in the z-direction. Now, to understand the effect of the electric force and the presence of ions on the structure in the x-y plane, we computed the radial distribution function in the x-y plane that is defined as

$$g_{//}(r)=\frac{1}{\rho^2 V}\sum_{i\neq j}\delta(r-r_{ij})\left[\theta\left(|z_i-z_j|-\frac{\delta z}{2}\right)-\theta\left(|z_i-z_j|+\frac{\delta z}{2}\right)\right] \quad (24)$$

where V is the volume, r_{ij} is distance parallel to the x-y plane between molecules i and j, z_i is the z coordinate and $\delta(x)$ is the Dirac delta function. The Heaviside function $\theta(x)$ restricts the sum to a pair molecules located in the same slab of width δz. The physical interpretation of $g_{//}(r)$ is that $g_{//}2\pi r dr\delta z$ is proportional to the probability of finding a molecule in a slab of thickness δz at a distance r parallel to the walls from a randomly chosen molecule. In a bulk liquid, this would be identical to g(r), the standard RDF.

Fig. 4 shows the radial distribution function of the molecules of the Lennard-Jones fluid and the center of water molecular mass of the pure water and the solution. The approximated long-range order indicates that the system has adopted the approximated crystalline phase. This can be explained by considering the Lennerd-Jones

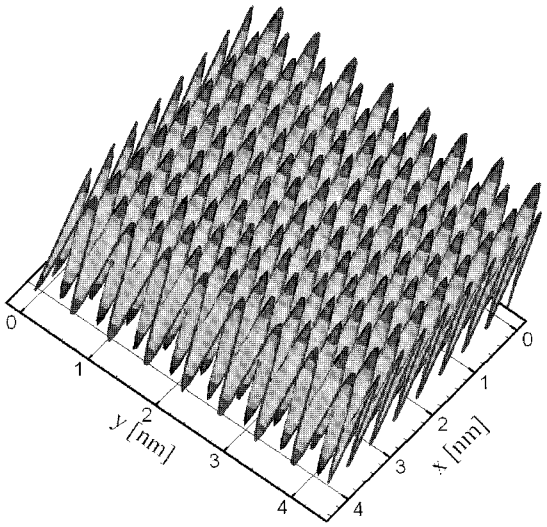

Fig. 5 The Lennard-Jones potential of the wall-water interaction in the x-y plane

potential between the fluid molecules and the wall(Fig. 5). We see that the distance between two long-range adjacent peaks in Fig. 4 is approximately equal to those in Fig. 5. This implies that the approximated crystalline phase is due to the walls. The difference of the radial distribution function for different fluids indicates that the electric force as well as the presence of ions in solution strongly affects this property of fluid.

C. Velocity Autocorrelation Function

We computed the velocity autocorrelation function to consider the dynamic property of the fluid confined in a slit channel. The autocorrelation function of a quantity X can be defined as

$$c_X(t) = \langle X(t)X(0) \rangle = \frac{1}{MN}\sum_{j=1}^{M}\sum_{i=1}^{N} X_i(t_j)X_i(t_j+t) \tag{25}$$

where M is the number of time origins and N is the number of molecules in the system. If the quantity X is velocity then autocorrelation function is the so-called velocity autocorrelation function(VACF).

Fig. 6 shows the x-y plane VACF and the z-direction VACF of fluid molecules in the channel. Both VACF's for the water fluid and the aqueous sodium-chloride

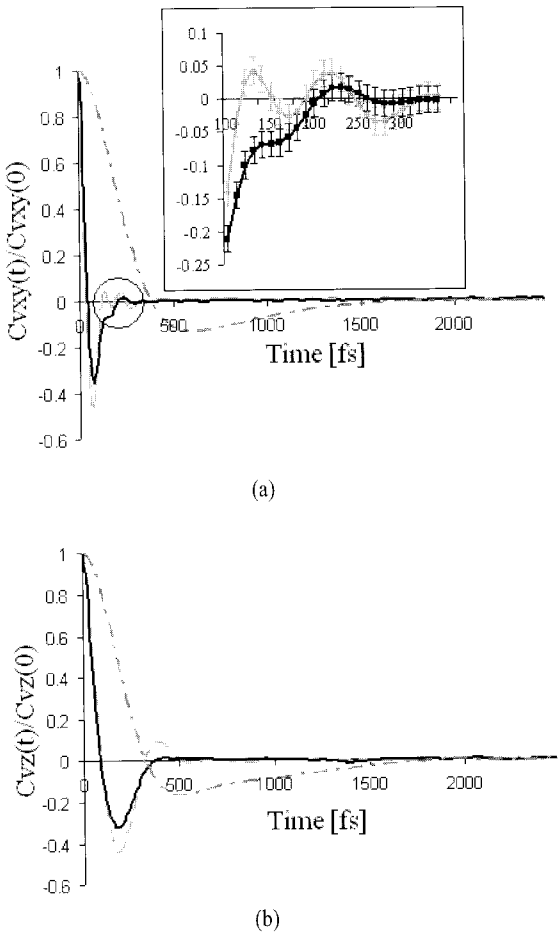

Fig. 6 The velocity autocorrelation functions of the fluid molecules, (a) $c_{vxy}(t)/c_{vxy}(0)$ and (b) $c_{vz}(t)/c_{vz}(0)$. Here, long dash, solid and dash dot lines indicate water, solution and Lennard-Jones fluids, respectively

solution cases initially rapidly decrease and then increase again compared to those in the Lennard-Jones fluid case. Further the minimum VACF of Lennar-Jones fluid is higher than that of the other fluids. This can be explained by considering firstly the number density and secondly possibly the influence of the electric force. As the first reason, we notice that for a higher number density the fluctuation of VACF becomes more pronounced[19]. As seen in the previous section, we see that the effective number densities for both electrolyte fluids, i.e., the water fluid and the aqueous sodium-chloride solution, are larger than that for the Lennard-Jones fluid. The second reason

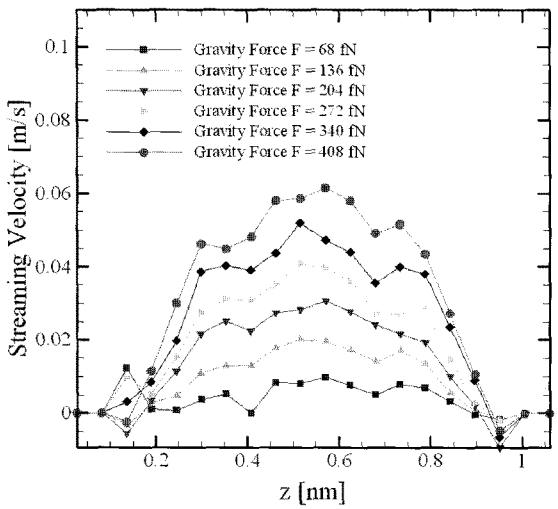

Fig. 7 The streaming velocity in the x-direction for different values of the gravity force for the Lennard-Jones fluid

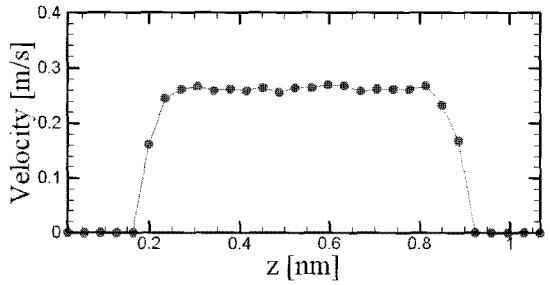

Fig. 8 The streaming velocity in the x-direction for the water

is that the interaction between fluid molecules is largely changed by adding the electric force that certainly leads to the change of motion of molecules. This indicates that the VACF of molecules are strongly affected by the electric force. From this figure, we also see that the difference between VACF's for the water and the solution is not so large. This implies that with the concentrations employed in this study the effect of the presence of ions on this property is weak.

D. The Velocity Profile and the Flow Rate

Next, the non-equilibrium molecular-dynamic simulations have been performed by applying a uniform gravity force parallel to the wall for both the Lennard-Jones fluid and the water. This case is similar to the case where the flow is created by applying a pressure gradient along the channel. In our study, the gravity force is related to the pressure gradient as follows.

$$F_{gravity} = \frac{\partial P}{\partial x} L_x (L_y L_z) \frac{1}{N} \tag{26}$$

To study the flow property in the nano-channel, we calculated the velocity profile from

$$\nu(z_n) = \frac{1}{M} \sum_{j=1}^{M} \frac{\sum_{i=1}^{N} H_n(z_{i,j}) \nu_{i,j}^x}{\sum_{j=1}^{N} H_n(z_{i,j})} \tag{27}$$

where, $z_n = (n-1/2)\Delta z$ and $H_n(z_{i,j})$ was given in Eq. (21).

Fig. 7 shows the velocity profile across the channel for different gravity forces for the Lennard-Jones fluid. Unexpectedly the velocity profiles are not parabolic. Each of the velocity profiles show two side lobes near roughly $z = 0.3$ and $z = 0.8$ in particular at high gravity forces. Travis et al.[1] also showed similar results. They computed the viscosity in these regions based on the mesoscopic method(i.e. from the balance between the pressure and shear forces) and the magnitude of the viscosity was so large compared to that in other regions. On the other hand, we see that regions of two side lobes are almost the same as those corresponding to two valleys in the number density profiles of Fig. 2(a). Thus we may think that possibly the number density could be related to the occurrence of two side lobes. However, those lobes are not so clear for the cases of small gravity force; this can be understood by the influence of statistical noise. The velocity close to wall is negative because of the statistical noise, too. Further, the velocity gradient is not so high near the wall, indicating that the non-wetting phenomenon does not occur for the L-J fluid contrary to the case of water as will be seen below.

Fig. 8 shows the velocity profile across the channel for the water. The velocity is almost uniform in the mid-channel and the velocity gradient is very high near the wall contrary to the L-J fluid. This implies that the non-wetting occurs in the channel. This can be understood as the influence of the electric force between water

molecules. The attractive interaction between fluid molecules is much stronger than the interaction between the fluid and wall molecules.

Next we calculated the flow rate defined as

$$Q_x = \int_{z_{bot}}^{z_{top}} \nu_x(z)dz \tag{28}$$

where z_{top} and z_{bot} denote the z-coordinates of the inner layers of the top and bottom walls, respectively. Fig. 9 shows the flow rate varied with the gravity force for the Lennard-Jones fluid. It indicates that the flow rate linearly increases with the gravity force with 95% confidence. This is consistent with the classical theory for fully-developed flow through a channel. By the way, it is unusual to confirm from the figure the non-zero gravity force at the zero flow rate. This is probably caused by the small ratio of the gravity force to the intermolecular force(in the order of 1%); for instance, Xu et al.[2] proposed three regimes as to the effect of the gravity force, the present case corresponding to the so called 'free molecule oscillation region' in which the gravity force actually has no effect on the flow.

4. CONCLUSIONS

We developed a FORTRAN code to perform MD simulation by using the Euler angles for the constraint of rigid molecules. The disadvantage of using the Euler angles in the MD simulation have been overcome by adding damping forces and moments to equations of molecular motion for proper setting of the initial configuration.

We addressed the effect of the electric force and the presence of ions on the statical as well as dynamical properties of the fluids that are confined in a nano-channel by using the equilibrium MD simulation; the channel width is set here at approximately 3 times the diameter of molecules. As for the number density profile, peaks adjacent to wall are not so distinctively different for three fluids, but the middle peaks for both the water and solution are much smaller than those of the Lennard-Jones fluid. To understand further about the statical property, we calculated the radial distribution functions and found that they are somewhat different for three kinds of fluids, and the fluids adopted the approximated crystalline phase by the influence of the walls. These indicate that the statical properties of fluid in the nano-channel are in general strongly influenced by the electric force and the presence of ions and the characteristic of the walls with one exceptional situation in which the density profile is weakly affected by the presence of ions. We estimated the effect of the electric force and the presence of ions on the dynamical property by computing the VACF. The VACF is similar to each other for the pure water and solution. However, the VACF of the Lennard-Jones fluid is different from that of the other two fluids. This implies that the electric force gives effects on the dynamical property but the presence of ions is relatively non-effective.

We carried out the non-equilibrium MD simulations for the Lennard-Jones fluid and water by applying gravity force to molecules. The velocity profiles for both fluids are not parabolic. For the Lennard-Jones fluid, the streaming velocity slowly tends to zero when the wall is approached, which may be considered as a symptom of the wetting phenomenon. However, the velocity profile for the water is almost uniform in the mid-channel and tends to zero so fast, which implies that the non-wetting phenomenon occurs for this case. Thus, the streaming velocity is strongly affected by the electric force. In addition, the dependence of the flow rate on the gravity force is evaluated by performing the non-equilibrium MD simulations for various gravity forces. We found that the flow rate is linearly dependent on the gravity force; this behavior is similar to that observed in the macro-channel.

ACKNOWLEDGEMENTS

This work was supported by the Korea Science and Engineering Foundation(KOSEF) through the National Research Laboratory Program funded by the Ministry of Science and Technology(No. 2005-1091)

REFERENCES

[1] 2000, Travis, K.P. and Gubbins, K.E., "Poiseuille flow of Lennard-Jones fluids in narrow slit pores," *J. Chem. Phys.*, Vol.112, p.1984.

[2] 2004, Xu, J.L. and Zhou, Z.Q., "Molecular dynamics

simulation of liquid argon flow at platinum surfaces," *Heat and Mass Transfer*, Vol.40, pp.859-869.

[3] 2005, Kumar, P., Buldyrev, S.V., Starr, F.W., Giovambattista, N. and Stanley, H.E., "Thermo-dynamics, structure, and dynamics of water confined between hydrophobic plates," *Phys. Rev. E.*, Vol.72, 051503.

[4] 2007, Kumar, P., Starr, F.W., Buldyrev, S.V. and Stanley, H.E., "Effect of water-wall interaction potential on the properties of nanoconfined water," *Phys. Rev. E.*, Vol.75, 011202.

[5] 2003, Zangi, R. and Mark, A.E., "Bilayer ice and alternate liquid phases of confined water," *J. Chem. Phys.*, Vol.119, p.1694.

[6] 2002, Qiao, R. and Alura, N.R., "Ion concentrations and velocity profiles in nanochannel electroosmotic flows," *J. Chem. Phys.*, Vol.118, p.4692.

[7] 2002, Freund, J.B., "Electro-osmosis in a nanometer-scale channel studied by atomistic simulation," *J. Chem. Phys.*, Vol.116, p.2194.

[8] 2006, Kim, D. and Darve, E., "Molecular dynamics simulation of electro-osmotic in rough wall nano-channel," *Phys. Rev. E.*, Vol.73, p.051203.

[9] 2008, Wang, M. and Chen. S., "On Applicability of Poisson-Boltzmann Equation for Micro- and Nanoscale Electro-osmotic Flows," *Common. Comput. Phys.*, Vol.3, pp.1087-1099.

[10] 2007, Kim, C.S., "Nonequilibrium Molecular Dynamics Approach for Nanoelectromechanical Systems: Nanofluidics and Its Applications," ASME, Vol.129, p.1140.

[11] 2005, Atamas, A.A., Atamas, N.A. and Bulavin, L.A., "Structure correlations of water molecules in a concentrated aqueous solution of ethanol," *J. Mol. Liq.*, Vol.120, pp.15-17.

[12] 2006, Brodka, A., "Optical parameter values of the Ewald method with electrostatic layer correction for Coulomb interactions in slab geometry," *J. Mol. Struc.*, Vol.792-793, pp.56-61.

[13] 1998, Deserno, M. and Holm, C., "How to mesh up Ewald sums (I): A theoretical and numerical comparison of various particle mesh routines," *J. Chem. Phys.*, Vol.109, p.7678.

[14] 1998, Deserno, M. and Holm, C., "How to mesh up Ewald sums. II. An accurate error estimate for the particle-particle-particle- mesh algorithm," *J. Chem. Phys.*, Vol.109, p.7694.

[15] 1999, Yeh, I.-C. and Berkowitz, M.L., "Ewald summation for systems with slab geometry," *J. Chem. Phys.*, Vol.111, p.3155.

[16] 2008, Hiyama, M., Kinjo, T. and Hyodo, S.A., "Angular Momentum Form of Verlet Algorithm for Rigid Molecules," *J. Phys. Soc. Japan*, Vol.77, 064001.

[17] 1992, Press, W.H., Teukolsky, S.A., Vetterling, W.T. and Flannery, B.P., *Numerical recipes in the Fortrans 77*, Cambridge University Press, Cambridge.

[18] 1987, Allen, M.P. and Tildesley, D.J., *Computer Simulation of Liquids*, Clarendon Press, Oxford.

[19] 1997, Haile, J.M., *Molecular Dynamcis Simulation*, Wiley-Interscience Press, USA.

[20] 1995, Rapaport, D.C., *The art of Molecular Dynamics Simulations*, Cambridge University Press, Cambridge.

[21] http://en.wikipedia.org/wiki/silic.